

# Complete Bell-state analysis for superconducting-quantum-interference-device qubits with a transitionless tracking algorithm

Yi-Hao Kang,<sup>1,2</sup> Ye-Hong Chen,<sup>1,2</sup> Zhi-Cheng Shi,<sup>1,2</sup> Bi-Hua Huang,<sup>1,2</sup> Jie Song,<sup>3</sup> and Yan Xia<sup>1,2,\*</sup>

<sup>1</sup>Department of Physics, Fuzhou University, Fuzhou 350116, China

<sup>2</sup>Fujian Key Laboratory of Quantum Information and Quantum Optics (Fuzhou University), Fuzhou 350116, China

<sup>3</sup>Department of Physics, Harbin Institute of Technology, Harbin 150001, China

(Received 12 June 2017; published 4 August 2017)

We propose a protocol for complete Bell-state analysis for two superconducting-quantum-interference-device qubits. The Bell-state analysis could be completed by using a sequence of microwave pulses designed by the transitionless tracking algorithm, which is a useful method in the technique of shortcut to adiabaticity. After the whole process, the information for distinguishing four Bell states will be encoded on two auxiliary qubits, while the Bell states remain unchanged. One can read out the information by detecting the auxiliary qubits. Thus the Bell-state analysis is nondestructive. The numerical simulations show that the protocol possesses a high success probability of distinguishing each Bell state with current experimental technology even when decoherence is taken into account. Thus, the protocol may have potential applications for the information readout in quantum communications and quantum computations in superconducting quantum networks.

DOI: 10.1103/PhysRevA.96.022304

## I. INTRODUCTION

Entanglement is a basic concept in quantum information science. It provides the possibility to test quantum nonlocality against local hidden theory [1–3] and also plays a key role in various quantum information tasks [4–10]. Therefore, preparing [11,12], transferring [13,14], and purifying [15,16] all kinds of entangled states in different physical systems have become hot topics in quantum information processing (QIP). As Bell states of two qubits are easy to be obtained and manipulated, they have been employed as the information carriers in quantum communications and quantum computations [6,8,17]. Thus, when using Bell states as information carriers, reading out quantum information encoded on Bell states is an indispensable task, which has greatly motivated the research on the Bell-state analysis. At the beginning, researchers mainly paid attention to the Bell-state analysis for polarized photons with linear optical elements [18,19]. But, unfortunately, it has been proven by protocols [20,21] that the Bell-state analysis with only the linear optical element has an optimal success probability of 0.5. Besides, the Bell-state analysis usually destroys the entanglement, which causes the waste of physical resources. Therefore, to achieve complete and nondestructive Bell-state analysis and to exploit the advantages of other physical systems, researchers have turned their attention to Bell states in various systems by applying many new techniques, such as nonlinearities and hyperentanglement. Until now, complete and nondestructive Bell-state analyses for photons [22–28], atoms [29], spins inside quantum dots [30,31], and nitrogen-vacancy centers [32] have been reported.

In recent years, the superconducting system has been developed a lot, and is now deemed as a very promising candidate to implement quantum information tasks [33–57], as it possesses many advantages. Superconducting qubits, including phase qubits, charge qubits, flux qubits, etc., are outstanding with their relatively long decoherence time [46] and perfect scal-

bility [35,36,39]. Among all kinds of superconducting qubits, the superconducting-quantum-interference-device (SQUID) qubits in cavity quantum electrodynamics (QED) have many advantages:

(1) The positions of SQUID qubits in a cavity are fixed. That makes them superior compared with neutral atoms, which require the centers-of-mass motion in a cavity to be controlled [37,38].

(2) When placing SQUID qubits into a superconducting cavity, decoherence induced by the external environment can be greatly suppressed since the superconducting cavity could be considered as the magnetic shield for SQUID qubits [38].

(3) The strong-coupling limit of the cavity QED can be easily realized for SQUID qubits embedded in a cavity, while it is difficult to be realized with atoms [37].

(4) The level structure of every individual SQUID qubit can be adjusted easily [37].

The great advantages of SQUID qubits make them attractive choices to implement quantum information tasks. So far, SQUID qubits have been widely used in entanglement preparations [11,37,38,58], information transfers [37,38], and logic gates [38]. However, Bell-state analysis for SQUID qubits still has plenty of room for research.

On the other hand, when choosing a superconducting system as the platform for QIP, an ineluctable question is to design microwave pulses driving superconducting qubits to complete various operations. Interestingly, a new technique called shortcut to adiabaticity (STA) [59–92] has been developing recently to control quantum evolutions. Rather than confining quantum evolutions along one eigenstate or superpositions of several eigenstates of the Hamiltonian under the adiabatic condition, STA provides a lot of evolution paths by means of various methods, including transitionless tracking algorithm [59–63], Lewis-Riesenfeld invariants theory [63,65], Lie algebra [69,70], picture transformations [74–77], fast-forward scales [81,82], etc. These protocols [59–92] have demonstrated that STA not only inherits the robustness of the adiabatic passage, but also greatly accelerates adiabatic processes. Moreover, constructing STA by using different

\*xia-208@163.com

methods produces excellent feasibility to handle all kinds of quantum information tasks. Thus, it may be a good idea to apply STA in pulse design to manipulate superconducting systems.

In this paper, motivated by (1) the importance of Bell-state analysis in quantum information tasks, (2) the advantages of SQUID qubits, (3) the requirement of Bell-state analysis from quantum communications and computations within superconducting quantum networks, and (4) the advantages of STA in designing pulses to control physical systems, we proposed a protocol for complete and nondestructive Bell-state analysis for two SQUID qubits. By using the transitionless tracking algorithm, a useful method of STA, a sequence of microwave pulses is designed to complete the Bell-state analysis. The information for distinguishing four Bell states would be encoded in two auxiliary SQUID qubits and could be read out with current technology [93,94]. Therefore, the operations of the Bell-state analysis are not difficult in real experiments. Besides, the protocol combines the robustness of SQUID qubits and the speediness of STA. Thus, we can see in numerical simulation that a high success probability to distinguish each Bell state is still available when decoherence is considered. By substituting experimentally realizable parameters, good performance of the Bell-state analysis is shown.

The article is organized as follows. In Sec. II, we briefly review the physical model of a SQUID qubit. In Sec. III, we amply illuminate the procedures of the Bell-state analysis. In Sec. IV, the transitionless tracking algorithm is utilized to design microwave pulses for realizing the Bell-state analysis. In Sec. V, numerical simulations are performed to select suitable control parameters and demonstrate the robustness of the Bell-state analysis against decoherence. Finally, conclusions are given in Sec. VI.

## II. PHYSICAL MODEL OF A SQUID QUBIT

Considering a single SQUID qubit with junction capacitance  $C$  and loop inductance  $L$ , its Hamiltonian reads [37,38]

$$H_s(t) = \frac{Q^2}{2C} + \frac{(\Phi - \Phi_x)^2}{2L} - E_J \cos\left(2\pi \frac{\Phi}{\Phi_0}\right), \quad (1)$$

where  $Q$  is the total charge on the capacitor,  $\Phi$  is the magnetic flux threading the loop, and  $\Phi_x$  is the external flux applied to the ring;  $E_J = I_c \Phi_0 / 2\pi$  is the Josephson energy with  $I_c$  and  $\Phi_0 = h/2e$  is the critical current of the junction and the flux quantum. By quantizing the Hamiltonian of the SQUID qubit, the SQUID qubit can be described by a level diagram with a serial of energy levels  $\{|k\rangle\}$  ( $k = 0, 1, 2, \dots$ ), shown in Fig. 1 [37,38]. When a transition between two different levels  $|k\rangle$  and  $|k'\rangle$  is driving by a classical microwave field, in the frame of the rotating-wave approximation, the Rabi frequency of the driving field could be written as [37,38]

$$\Omega_{kk'}(t) = \frac{1}{2L\hbar} \langle k | \Phi | k' \rangle \int_S \tilde{\mathbf{B}}_{\mu w}(\mathbf{r}, t) \cdot d\mathbf{S}, \quad (2)$$

where  $S$  is the surface bounded by the loop of the SQUID qubit;  $\tilde{\mathbf{B}}_{\mu w}(\mathbf{r}, t) = \tilde{\mathbf{B}}_{\mu w}(\mathbf{r}, t) \cos(2\pi v_{\mu w} t)$  is the magnetic components of the classical microwave in the superconducting loop of the SQUID qubit with frequency  $v_{\mu w}$ . Considering that the SQUID qubit is placed in a microwave cavity, when a

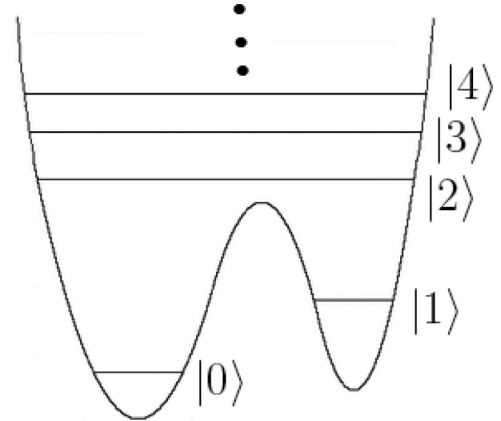


FIG. 1. The level configuration of a single SQUID qubit.

transition between two different levels  $|k\rangle$  and  $|k'\rangle$  is coupled to a quantized cavity field with frequency  $\omega_c$ , after the rotating-wave approximation, the coupling constant reads [37,38]

$$g_{kk'} = \frac{1}{L} \sqrt{\frac{\omega_c}{2\mu_0\hbar}} \langle k | \Phi | k' \rangle \int_S \mathbf{B}_c(\mathbf{r}) \cdot d\mathbf{S}, \quad (3)$$

where  $\mathbf{B}_c(\mathbf{r})$  is the magnetic components of the cavity mode in the superconducting loop of the SQUID qubit.

## III. COMPLETE BELL-STATE ANALYSIS

Consider a system that contains four SQUID qubits  $A_1, A_2, B_1, B_2$  placed inside a microwave cavity, which is shown in Fig. 2(a). SQUID qubit  $A_j$  ( $j = 1, 2$ ) is employed as an auxiliary qubit, whose level diagram is shown in Fig. 2(b). We consider the lowest five levels  $|0\rangle_{A_j}, |1\rangle_{A_j}, |2\rangle_{A_j}, |3\rangle_{A_j}$ , and  $|4\rangle_{A_j}$  of SQUID qubit  $A_j$ . The transition between  $|0\rangle_{A_j}$  and  $|3\rangle_{A_j}$  ( $|4\rangle_{A_j}$ ) is resonantly driven by a classical microwave field with Rabi frequency  $\Omega_{03A_j}(t)$  ( $\Omega_{04A_j}(t)$ ). The transition between  $|1\rangle_{A_j}$  and  $|3\rangle_{A_j}$  ( $|4\rangle_{A_j}$ ) is resonantly driven by a classical microwave field with Rabi frequency  $\Omega_{13A_j}(t)$  ( $\Omega_{14A_j}(t)$ ). SQUID qubits  $B_1$  and  $B_2$  are information carriers, whose level diagrams are shown in Fig. 2(c). We consider the lowest three levels  $|0\rangle_{B_j}, |1\rangle_{B_j}, |2\rangle_{B_j}$  and among them, information is encoded on  $|0\rangle_{B_j}$  and  $|1\rangle_{B_j}$ . Thus, the four Bell states to be distinguished can be described as

$$\begin{aligned} |\Psi_{\pm}\rangle_{B_1B_2} &= \frac{1}{\sqrt{2}} (|0\rangle_{B_1}|0\rangle_{B_2} \pm |1\rangle_{B_1}|1\rangle_{B_2}), \\ |\Phi_{\pm}\rangle_{B_1B_2} &= \frac{1}{\sqrt{2}} (|0\rangle_{B_1}|1\rangle_{B_2} \pm |1\rangle_{B_1}|0\rangle_{B_2}). \end{aligned} \quad (4)$$

A classical microwave field with Rabi frequency  $\Omega_{B_j}(t)$  is applied on SQUID qubit  $B_j$  to drive the transition between levels  $|0\rangle_{B_j}$  and  $|1\rangle_{B_j}$ . Assume the microwave cavity is a double-mode cavity, where two cavity fields  $a_1$  and  $a_2$  (denoted by their annihilation operators) may exist. The cavity field  $a_1$  ( $a_2$ ) could resonantly couple with the transition between levels  $|2\rangle_{A_j}$  ( $j = 1, 2$ ) and  $|3\rangle_{A_j}$  ( $|2\rangle_{A_j}$  and  $|4\rangle_{A_j}$ ) of SQUID qubit  $A_j$  with coupling constant  $g_{23A_j}$  ( $g_{24A_j}$ ), and the transition between levels  $|0\rangle_{B_1}$  and  $|2\rangle_{B_1}$  ( $|0\rangle_{B_2}$  and  $|2\rangle_{B_2}$ ) with coupling constant  $g_{B_1}$  ( $g_{B_2}$ ). Assume the frequencies of cavity modes  $a_1$  and  $a_2$  are  $\omega_1$  and  $\omega_2$ , respectively. The transition frequency

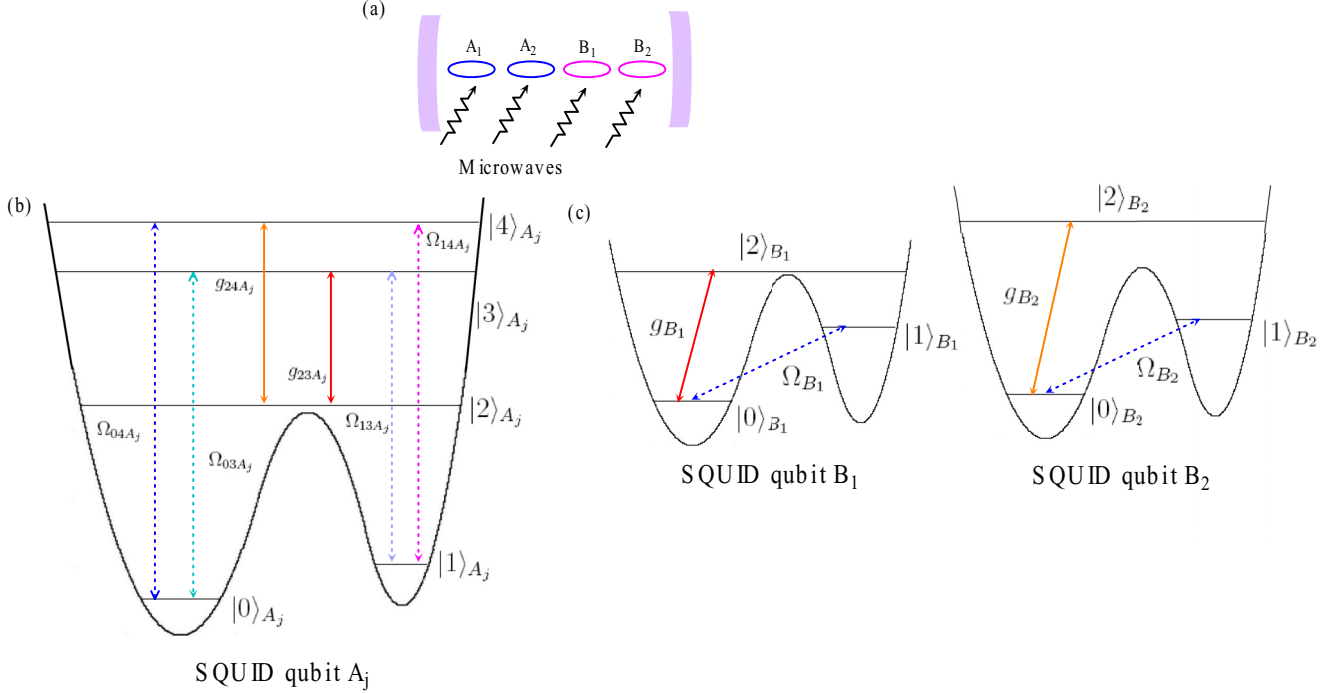


FIG. 2. (a) The auxiliary qubits \$A\_1\$, \$A\_2\$ and the information carriers \$B\_1\$, \$B\_2\$ placed in a microwave cavity. (b) The level configuration of SQUID qubit \$A\_j\$ (\$j = 1, 2\$). (c) The level configurations of SQUID qubits \$B\_1\$ and \$B\_2\$.

between \$|0\rangle\_{B\_1}\$ and \$|2\rangle\_{B\_1}\$ (\$|0\rangle\_{B\_2}\$ and \$|2\rangle\_{B\_2}\$) of SQUID qubit \$B\_1\$ (\$B\_2\$) should be equal to \$\omega\_1\$ (\$\omega\_2\$). According to Ref. [37], the level structure of each individual SQUID qubit can be adjusted by either design variations and/or changing the local bias field. Thus, coupling between microwave pulses (cavity fields) and any particular SQUID qubits can be obtained selectively via frequency matching. When \$g\_{B\_1}, g\_{B\_2} \ll |\omega\_1 - \omega\_2|\$, the interaction between SQUID qubit \$B\_1\$ and cavity mode \$a\_2\$ (SQUID qubit \$B\_2\$ and cavity mode \$a\_1\$) could be discarded [38]. Therefore, in the interaction picture, the total Hamiltonian of the system for the Bell-state analysis could be written as

$$\begin{aligned}
 H_I(t) &= H_{mA}(t) + H_{mB} + H_c, \\
 H_{mA}(t) &= \sum_{j=1,2} \Omega_{03A_j}(t) |0\rangle\langle 3| + \Omega_{04A_j}(t) |0\rangle\langle 4| \\
 &\quad \times \langle 4| + \Omega_{13A_j}(t) |1\rangle\langle 3| + \Omega_{14A_j}(t) |1\rangle\langle 4| + \text{H.c.}, \\
 H_{mB}(t) &= \sum_{j=1,2} \Omega_{B_j}(t) e^{-i\epsilon_j} |0\rangle\langle 1| + \text{H.c.}, \\
 H_c &= \sum_{j=1,2} g_{23A_j} |3\rangle_{A_j}\langle 2| a_1 + g_{24A_j} |4\rangle_{A_j}\langle 2| a_2 + g_{B_j} |2\rangle_{B_j} \\
 &\quad \times \langle 0| a_j + \text{H.c.}, \tag{5}
 \end{aligned}$$

where \$\epsilon\_j\$ is the phase shift of \$\Omega\_{B\_j}\$. Here, we take \$\epsilon\_j = \pi/2\$ for the convenience of calculations and descriptions.

Now, let us describe the procedures for Bell-state analysis. The Bell state can be divided into six steps. We do not discuss the pulse design here, but leave it until later in Sec. IV. Besides, for the convenience of descriptions, we assume the operation time of each step is \$T\$.

*Step 1.* Assume SQUID qubit \$A\_j\$ is initially in state \$|0\rangle\_{A\_j}\$, and cavity field \$a\_j\$ is initially in vacuum state \$|0\rangle\_{a\_j}\$. We turn on \$\Omega\_{03A\_1}(t)\$ and \$\Omega\_{13A\_1}(t)\$, but turn off other classical microwave fields. In this case, SQUID qubit \$A\_2\$ is decoupled to the system. In addition, cavity fields \$a\_2\$ keep in a vacuum state. Thus, whether SQUID qubit \$B\_2\$ is in state \$|0\rangle\_{B\_2}\$ or \$|1\rangle\_{B\_2}\$, it does not evolve as well. Without considering cavity field \$a\_2\$ and the decoupled SQUID qubits, the system would evolve in a subspace spanned by

$$\begin{aligned}
 |\bar{\psi}_1\rangle &= |0\rangle_{A_1}|0\rangle_{B_1}|0\rangle_{a_1}, \quad |\bar{\psi}_2\rangle = |3\rangle_{A_1}|0\rangle_{B_1}|0\rangle_{a_1}, \\
 |\bar{\psi}_3\rangle &= |2\rangle_{A_1}|0\rangle_{B_1}|1\rangle_{a_1}, \\
 |\bar{\psi}_4\rangle &= |2\rangle_{A_1}|2\rangle_{B_1}|0\rangle_{a_1}, \quad |\bar{\psi}_5\rangle = |1\rangle_{A_1}|0\rangle_{B_1}|0\rangle_{a_1}, \\
 |\bar{\psi}_6\rangle &= |0\rangle_{A_1}|1\rangle_{B_1}|0\rangle_{a_1}, \\
 |\bar{\psi}_7\rangle &= |3\rangle_{A_1}|1\rangle_{B_1}|0\rangle_{a_1}, \quad |\bar{\psi}_8\rangle = |2\rangle_{A_1}|1\rangle_{B_1}|1\rangle_{a_1}, \\
 |\bar{\psi}_9\rangle &= |1\rangle_{A_1}|1\rangle_{B_1}|0\rangle_{a_1}, \tag{6}
 \end{aligned}$$

where \$|1\rangle\_{a\_1}\$ denotes the one-photon state of cavity field \$a\_1\$. Rewriting the Hamiltonian of the system within the subspace, we obtain

$$\begin{aligned}
 H_{step1}(t) &= H_{m1}(t) + H_{c1}, \\
 H_{m1}(t) &= \Omega_{03A_1}(t)(|\bar{\psi}_1\rangle\langle\bar{\psi}_2| + |\bar{\psi}_6\rangle\langle\bar{\psi}_7|) \\
 &\quad + \Omega_{13A_1}(t)(|\bar{\psi}_5\rangle\langle\bar{\psi}_2| + |\bar{\psi}_9\rangle\langle\bar{\psi}_7|) + \text{H.c.}, \\
 H_{c1} &= g_{23A_1}(|\bar{\psi}_2\rangle\langle\bar{\psi}_3| + |\bar{\psi}_7\rangle\langle\bar{\psi}_8|) \\
 &\quad + g_{B_1}|\bar{\psi}_4\rangle_{B_1}\langle\bar{\psi}_3| + \text{H.c.} \tag{7}
 \end{aligned}$$

The eigenstates of  $H_{c1}$  are

$$\begin{aligned} |\tilde{\phi}_0\rangle &= \frac{1}{\sqrt{g_{23A_1}^2 + g_{B_1}^2}}(g_{B_1}|\tilde{\psi}_2\rangle - g_{23A_1}|\tilde{\psi}_4\rangle), \\ |\tilde{\phi}_1\rangle &= \frac{1}{\sqrt{2}}(|\tilde{\psi}_7\rangle + |\tilde{\psi}_8\rangle), \\ |\tilde{\phi}_2\rangle &= \frac{1}{\sqrt{2}}(|\tilde{\psi}_7\rangle - |\tilde{\psi}_8\rangle), \\ |\tilde{\phi}_3\rangle &= \frac{1}{\sqrt{2(g_{23A_1}^2 + g_{B_1}^2)}}(g_{23A_1}|\tilde{\psi}_2\rangle \\ &\quad + \sqrt{g_{23A_1}^2 + g_{B_1}^2}|\tilde{\psi}_3\rangle + g_{B_1}|\tilde{\psi}_4\rangle), \\ |\tilde{\phi}_4\rangle &= \frac{1}{\sqrt{2(g_{23A_1}^2 + g_{B_1}^2)}}(g_{23A_1}|\tilde{\psi}_2\rangle \\ &\quad - \sqrt{g_{23A_1}^2 + g_{B_1}^2}|\tilde{\psi}_3\rangle + g_{B_1}|\tilde{\psi}_4\rangle), \end{aligned} \quad (8)$$

with corresponding eigenvalues  $0$ ,  $g_{23A_1}$ ,  $-g_{23A_1}$ ,  $\sqrt{g_{23A_1}^2 + g_{B_1}^2}$ , and  $-\sqrt{g_{23A_1}^2 + g_{B_1}^2}$ , respectively. With the condition  $\Omega_{03A_1}(t), \Omega_{13A_1}(t) \ll g_{23A_1}, g_{B_1}$ , we can derive the effective Hamiltonian of the system as

$$\begin{aligned} H_{\text{eff}1}(t) &= \frac{g_{B_1}}{\sqrt{g_{23A_1}^2 + g_{B_1}^2}}[\Omega_{03A_1}(t)|\tilde{\psi}_1\rangle\langle\tilde{\phi}_0| \\ &\quad + \Omega_{13A_1}(t)|\tilde{\psi}_5\rangle\langle\tilde{\phi}_0|] + \text{H.c.} \end{aligned} \quad (9)$$

The details of the derivation of  $H_{\text{eff}1}(t)$  are given in the Appendix. To realize  $|\tilde{\psi}_1\rangle \rightarrow |\tilde{\psi}_5\rangle$ , we should suitably design  $\Omega_{03A_1}(t)$  and  $\Omega_{13A_1}(t)$ . The design of  $\Omega_{03A_1}(t)$  and  $\Omega_{13A_1}(t)$  is amply discussed in Sec. IV. Thus, if SQUID qubit  $B_1$  is initially in state  $|0\rangle_{B_1}$ , after Step 1, its state remains unchanged, while SQUID qubit  $A_1$  evolves from  $|0\rangle_{A_1}$  to  $|1\rangle_{A_1}$ . But if qubit  $B_1$  is initially in state  $|1\rangle_{B_1}$ , both SQUID qubits  $A_1$  and  $B_1$  remain in their initial states after Step 1.

**Step 2.** In this step, we turn on  $\Omega_{04A_1}(t)$  and  $\Omega_{14A_1}(t)$ , but turn off other classical microwave fields. Similar to Step 1, SQUID qubit  $A_2$  is decoupled to the system, while cavity fields  $a_1$  remain in a vacuum state. Thus, SQUID qubit  $B_1$  is decoupled to the system in this step. The system would evolve in a subspace spanned by

$$\begin{aligned} |\tilde{\psi}_1\rangle &= |0\rangle_{A_1}|0\rangle_{B_2}|0\rangle_{a_2}, \quad |\tilde{\psi}_2\rangle = |4\rangle_{A_1}|0\rangle_{B_2}|0\rangle_{a_2}, \\ |\tilde{\psi}_3\rangle &= |2\rangle_{A_1}|0\rangle_{B_2}|1\rangle_{a_2}, \\ |\tilde{\psi}_4\rangle &= |2\rangle_{A_1}|2\rangle_{B_2}|0\rangle_{a_2}, \quad |\tilde{\psi}_5\rangle = |1\rangle_{A_1}|0\rangle_{B_2}|0\rangle_{a_2}, \\ |\tilde{\psi}_6\rangle &= |0\rangle_{A_1}|1\rangle_{B_2}|0\rangle_{a_2}, \\ |\tilde{\psi}_7\rangle &= |4\rangle_{A_1}|1\rangle_{B_2}|0\rangle_{a_2}, \quad |\tilde{\psi}_8\rangle = |2\rangle_{A_1}|1\rangle_{B_2}|1\rangle_{a_2}, \\ |\tilde{\psi}_9\rangle &= |1\rangle_{A_1}|1\rangle_{B_2}|0\rangle_{a_2}. \end{aligned} \quad (10)$$

In a similar way, under the condition  $\Omega_{04A_1}(t), \Omega_{14A_1}(t) \ll g_{24A_1}, g_{B_2}$ , the effective Hamiltonian of the system can be derived as

$$\begin{aligned} H_{\text{eff}2}(t) &= \frac{g_{B_2}}{\sqrt{g_{24A_1}^2 + g_{B_2}^2}}[\Omega_{04A_1}(t)|\tilde{\psi}_1\rangle\langle\tilde{\phi}_0| \\ &\quad + \Omega_{14A_1}(t)|\tilde{\psi}_5\rangle\langle\tilde{\phi}_0|] + \text{H.c.} \end{aligned} \quad (11)$$

TABLE I. The evolution of  $A_1$  in Step 1 and Step 2.

The state of $B_1$ and $B_2$	Step 1	Step 2
$ 0\rangle_{B_1} 0\rangle_{B_2}$	$ 0\rangle_{A_1} \rightarrow  1\rangle_{A_1}$	$ 1\rangle_{A_1} \rightarrow  0\rangle_{A_1}$
$ 0\rangle_{B_1} 1\rangle_{B_2}$	$ 0\rangle_{A_1} \rightarrow  1\rangle_{A_1}$	$ 1\rangle_{A_1} \rightarrow  1\rangle_{A_1}$
$ 1\rangle_{B_1} 0\rangle_{B_2}$	$ 0\rangle_{A_1} \rightarrow  0\rangle_{A_1}$	$ 0\rangle_{A_1} \rightarrow  1\rangle_{A_1}$
$ 1\rangle_{B_1} 1\rangle_{B_2}$	$ 0\rangle_{A_1} \rightarrow  0\rangle_{A_1}$	$ 0\rangle_{A_1} \rightarrow  0\rangle_{A_1}$

with  $|\tilde{\phi}_0\rangle = \frac{1}{\sqrt{g_{24A_1}^2 + g_{B_2}^2}}(g_{B_2}|\tilde{\psi}_2\rangle - g_{24A_1}|\tilde{\psi}_4\rangle)$ . The design of  $\Omega_{04A_1}(t)$  and  $\Omega_{14A_1}(t)$  for achieving  $|\tilde{\psi}_1\rangle \leftrightarrow |\tilde{\psi}_5\rangle$  is also discussed in Sec. IV. Therefore, if SQUID qubit  $B_2$  is initially in state  $|0\rangle_{B_2}$ , its state keeps unchanged, while the evolution of SQUID qubit  $A_1$  would be  $|0\rangle_{A_1} \rightarrow |1\rangle_{A_1}$  or  $|1\rangle_{A_1} \rightarrow |0\rangle_{A_1}$ , where the initial state of SQUID qubit  $A_1$  in this step is decided by the result of Step 1. Otherwise, the initial state of SQUID qubit  $B_2$  is  $|1\rangle_{B_2}$ , and both SQUID qubits  $A_1$  and  $B_2$  stay in their initial states.

Step 1 and Step 2 are summarized in Table I.

Thus, after Step 1 and Step 2, information for distinguishing  $|\Psi_{\pm}\rangle_{B_1B_2}$  from  $|\Phi_{\pm}\rangle_{B_1B_2}$  is encoded on the SQUID qubit  $A_1$ .

**Step 3.** In this step, we only turn on classical microwave fields  $\Omega_{B_1}(t)$  and  $\Omega_{B_2}(t)$  to perform single-qubit operation on SQUID qubits  $B_1$  and  $B_2$ . When

$$\int_{2T}^{3T} \Omega_{B_j}(t')dt' = \pi/4, \quad (12)$$

the single-qubit operation on SQUID qubit  $B_j$  is

$$\begin{aligned} |0\rangle_{B_j} &\rightarrow \frac{1}{\sqrt{2}}(|0\rangle_{B_j} + |1\rangle_{B_j}), \\ |1\rangle_{B_j} &\rightarrow -\frac{1}{\sqrt{2}}(|0\rangle_{B_j} - |1\rangle_{B_j}). \end{aligned} \quad (13)$$

Therefore, the four Bell states change as follows:

$$\begin{aligned} |\Psi_+\rangle_{B_1B_2} &\rightarrow |\Psi_+\rangle_{B_1B_2}, \quad |\Psi_-\rangle_{B_1B_2} \rightarrow |\Phi_+\rangle_{B_1B_2}, \\ |\Phi_+\rangle_{B_1B_2} &\rightarrow -|\Psi_-\rangle_{B_1B_2}, \quad |\Phi_-\rangle_{B_1B_2} \rightarrow |\Phi_-\rangle_{B_1B_2}. \end{aligned} \quad (14)$$

Thus, we can transform the question of distinguishing  $|\Psi_+\rangle_{B_1B_2}$  ( $|\Phi_+\rangle_{B_1B_2}$ ) from  $|\Psi_-\rangle_{B_1B_2}$  ( $|\Phi_-\rangle_{B_1B_2}$ ) to the question of distinguishing  $|\Psi_{\pm}\rangle_{B_1B_2}$  from  $|\Phi_{\pm}\rangle_{B_1B_2}$ .

**Step 4.** We turn on  $\Omega_{03A_2}(t)$  and  $\Omega_{13A_2}(t)$ , but turn off other classical microwave fields. In this step, SQUID qubit  $A_2$  takes the place of SQUID qubit  $A_1$  in Step 1. Thus, by suitably designing  $\Omega_{03A_2}(t)$  and  $\Omega_{13A_2}(t)$ , we can make SQUID qubit  $A_2$  evolve from  $|0\rangle_{A_2}$  to  $|1\rangle_{A_2}$  when SQUID qubit  $B_1$  is in state  $|0\rangle_{B_1}$ , while remaining in  $|0\rangle_{A_2}$  when qubit  $B_1$  is in state  $|1\rangle_{B_1}$ .

**Step 5.** We only turn on  $\Omega_{04A_2}(t)$  and  $\Omega_{14A_2}(t)$ . In this step, SQUID qubit  $A_2$  takes the place of SQUID qubit  $A_1$  in Step 2. Therefore, with suitable  $\Omega_{04A_2}(t)$  and  $\Omega_{14A_2}(t)$ , we can also make SQUID qubit  $A_2$  evolve from  $|0\rangle_{A_2}$  to  $|1\rangle_{A_2}$  ( $|1\rangle_{A_2}$  to  $|0\rangle_{A_2}$ ) when SQUID qubit  $B_2$  is in state  $|0\rangle_{B_2}$ , while remaining in  $|0\rangle_{A_2}$  when qubit  $B_2$  is in state  $|1\rangle_{B_2}$ . After Step 4 and Step 5, the information for distinguishing  $|\Psi_+\rangle_{B_1B_2}$  ( $|\Phi_+\rangle_{B_1B_2}$ ) from  $|\Psi_-\rangle_{B_1B_2}$  ( $|\Phi_-\rangle_{B_1B_2}$ ) is encoded on SQUID qubit  $A_2$ .

**Step 6.** In this step, we only turn on classical microwave fields  $\Omega_{B_1}(t)$  and  $\Omega_{B_2}(t)$  to perform inverse transformations of

TABLE II. Measurement results of the states of SQUID qubits  $A_1$  and  $A_2$  with the corresponding Bell states of  $B_1$  and  $B_2$ .

Measurement result	Corresponding Bell state
$ 0\rangle_{A_1} 0\rangle_{A_2}$	$ \Psi_+\rangle_{B_1B_2}$
$ 0\rangle_{A_1} 1\rangle_{A_2}$	$ \Psi_-\rangle_{B_1B_2}$
$ 1\rangle_{A_1} 0\rangle_{A_2}$	$ \Phi_+\rangle_{B_1B_2}$
$ 1\rangle_{A_1} 1\rangle_{A_2}$	$ \Phi_-\rangle_{B_1B_2}$

Step 3 on SQUID qubits  $B_1$  and  $B_2$ . When

$$\int_{5T}^{6T} \Omega_{B_j}(t') dt' = -\pi/4, \quad (15)$$

the transformations for SQUID qubit  $B_j$  are

$$|0\rangle_{B_j} \rightarrow \frac{1}{\sqrt{2}}(|0\rangle_{B_j} - |1\rangle_{B_j}), \quad |1\rangle_{B_j} \rightarrow \frac{1}{\sqrt{2}}(|0\rangle_{B_j} + |1\rangle_{B_j}). \quad (16)$$

After that, the states of SQUID qubits  $B_1$  and  $B_2$  recover to their initial forms.

At the end of the Bell-state analysis, we detect the states of SQUID qubits  $A_1$  and  $A_2$ , thus reading out the information for distinguishing the four Bell states of SQUID qubits  $B_1$  and  $B_2$ . The measurement results of the states of SQUID qubits  $A_1$  and  $A_2$  with the corresponding Bell state of SQUID qubits  $B_1$  and  $B_2$  are shown in Table II. According to measurement results of the states of SQUID qubits  $A_1$  and  $A_2$ , a complete and nondestructive Bell-state analysis can be realized.

#### IV. PULSE DESIGN VIA STA

In this section, let us design the microwave pulse via STA. As we can see from Sec. III, the effective Hamiltonians of Steps 1, 2, 4, and 5 of the Bell-state analysis have the form

$$H(t) = \Omega_1(t)|\psi_1\rangle\langle\psi_2| + \Omega_2(t)|\psi_2\rangle\langle\psi_3| + \text{H.c.} \quad (17)$$

The required transformation is  $|\psi_1\rangle \leftrightarrow |\psi_3\rangle$ . Here, to build up evolution paths, we consider the transitionless tracking algorithm. It is pointed out by Ref. [62] that while utilizing the transitionless tracking algorithm, not only the eigenstates of the Hamiltonian but also a set of orthonormalized time-dependent vectors can be selected as the evolution paths. For the current protocol, we select

$$\begin{aligned} |\xi_1(t)\rangle &= (\cos\theta\sin\varphi\cos\vartheta + \sin\theta\sin\vartheta)|\psi_1\rangle \\ &\quad + i\cos\varphi\cos\vartheta|\psi_2\rangle + (\sin\theta\sin\varphi\cos\vartheta \\ &\quad - \cos\theta\sin\vartheta)|\psi_3\rangle, \\ |\xi_2(t)\rangle &= (\cos\theta\sin\varphi\sin\vartheta - \sin\theta\cos\vartheta)|\psi_1\rangle \\ &\quad + i\cos\varphi\sin\vartheta|\psi_2\rangle + (\sin\theta\sin\varphi\sin\vartheta \\ &\quad + \cos\theta\cos\vartheta)|\psi_3\rangle, \\ |\xi_3(t)\rangle &= \cos\theta\cos\varphi|\psi_1\rangle - i\sin\varphi|\psi_2\rangle + \sin\theta\cos\varphi|\psi_3\rangle, \end{aligned} \quad (18)$$

where,  $\theta$ ,  $\varphi$ , and  $\vartheta$  are three time-dependent parameters. According to the transitionless tracking algorithm, the evolution operator and the Hamiltonian for the evolution paths shown in

Eq. (18) could be derived by

$$U'(t) = \sum_{n=1}^3 |\xi_n(t)\rangle\langle\xi_n(0)|, \quad (19)$$

and

$$\begin{aligned} H'(t) &= i \sum_{n=1}^3 |\dot{\xi}_n(t)\rangle\langle\xi_n(t)| \\ &= (\dot{\varphi}\cos\theta + \dot{\vartheta}\sin\theta\cos\varphi)|\psi_1\rangle\langle\psi_2| \\ &\quad + (\dot{\varphi}\sin\theta - \dot{\vartheta}\cos\theta\cos\varphi)|\psi_2\rangle\langle\psi_3| \\ &\quad + i(\dot{\theta} - \dot{\vartheta}\sin\varphi)|\psi_3\rangle\langle\psi_1| + \text{H.c.} \end{aligned} \quad (20)$$

To make  $H'(t) = H(t)$ , it requires

$$\begin{aligned} \Omega_1(t) &= \dot{\varphi}\cos\theta + \dot{\vartheta}\sin\theta\cos\varphi, \\ \Omega_2(t) &= \dot{\varphi}\sin\theta - \dot{\vartheta}\cos\theta\cos\varphi, \\ \dot{\theta} &= \dot{\vartheta}\sin\varphi. \end{aligned} \quad (21)$$

Considering the time interval  $[0, T]$  and the boundary condition  $\varphi(0) = -\pi/2$ ,  $\varphi(T) = \pi/2$ ,  $\vartheta(0) + \theta(0) = 0$ , and  $\vartheta(T) - \theta(T) = \pi/2$ , we have  $U'(0) = I$  ( $I$  is the identical operator) and  $U'(T) = |\psi_1\rangle\langle\psi_3| + |\psi_3\rangle\langle\psi_1| + |\psi_2\rangle\langle\psi_2|$ . Thus, we can complete the transformation  $|\psi_1\rangle \leftrightarrow |\psi_3\rangle$ . With the boundary condition and Eq. (21), parameters  $\theta$ ,  $\vartheta$ , and  $\varphi$  can be selected to be

$$\varphi = -\frac{\pi}{2}\cos\left(\frac{\pi t}{T}\right), \quad \vartheta = \pi/4, \quad \theta = -\pi/4. \quad (22)$$

Then,  $\Omega_1(t)$  and  $\Omega_2(t)$  could be derived as

$$\Omega_1(t) = \frac{\pi^2}{2\sqrt{2}T} \sin(\pi t/T), \quad \Omega_2(t) = -\frac{\pi^2}{2\sqrt{2}T} \sin(\pi t/T). \quad (23)$$

Therefore, if we set

$$\begin{aligned} \Omega_{03A_1}(t) &= \frac{\sqrt{g_{23A_1}^2 + g_{B_1}^2}}{g_{B_1}} \Omega_1(t), \\ \Omega_{13A_1}(t) &= \frac{\sqrt{g_{23A_1}^2 + g_{B_1}^2}}{g_{B_1}} \Omega_2(t), \\ \Omega_{04A_1}(t-T) &= \frac{\sqrt{g_{24A_1}^2 + g_{B_2}^2}}{g_{B_2}} \Omega_1(t), \\ \Omega_{14A_1}(t-T) &= \frac{\sqrt{g_{24A_1}^2 + g_{B_2}^2}}{g_{B_2}} \Omega_2(t), \\ \Omega_{03A_2}(t-3T) &= \frac{\sqrt{g_{23A_2}^2 + g_{B_1}^2}}{g_{B_1}} \Omega_1(t), \\ \Omega_{13A_2}(t-3T) &= \frac{\sqrt{g_{23A_2}^2 + g_{B_1}^2}}{g_{B_1}} \Omega_2(t), \end{aligned}$$

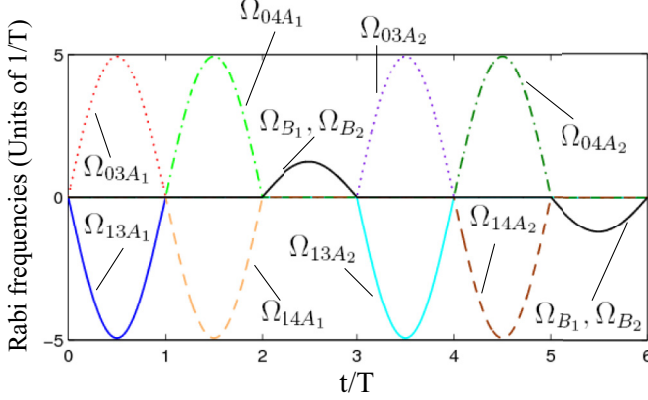


FIG. 3. Microwave pulses for the Bell-state analysis.

$$\Omega_{04A_2}(t - 4T) = \frac{\sqrt{g_{24A_2}^2 + g_{B_2}^2}}{g_{B_2}} \Omega_1(t),$$

$$\Omega_{14A_2}(t - 4T) = \frac{\sqrt{g_{24A_2}^2 + g_{B_2}^2}}{g_{B_2}} \Omega_2(t), \quad (24)$$

the microwave pulses could be used in the Bell-state analysis.

As for the  $\Omega_{B_j}(t)$ , which is used to perform a single-qubit operation on SQUID qubit  $B_j$  in Step 3, according to Eq. (12), it could be chosen as

$$\Omega_{B_j}(t - 2T) = \frac{\pi^2}{8T} \sin(\pi t/T). \quad (25)$$

Similarly, for  $\Omega_{B_j}(t)$ , which is used to perform a single-qubit operation on SQUID qubit  $B_j$  in Step 6, according to Eq. (15), it could be chosen as

$$\Omega_{B_j}(t - 5T) = -\frac{\pi^2}{8T} \sin(\pi t/T). \quad (26)$$

For simplicity, we consider  $g_{23A_j} = g_{24A_j} = g_{B_j} = g$ . The microwave pulses for the Bell-state analysis are shown in Fig. 3. The maximal value of the amplitudes of the pulses  $\Omega_{\max} = \pi^2/2T \simeq 4.9348/T$ .

## V. NUMERICAL SIMULATIONS

In this section, the robustness of the protocol is checked via numerical simulations. Before the numerical simulations, we first define the success probability for distinguishing each Bell state. Assume that the density operator of the system is  $\rho(t)$ . According to Table II, the success probabilities could be defined as

$$P(\Psi_+) = \langle 00\Psi_+ | \rho(6T) | 00\Psi_+ \rangle,$$

$$P(\Psi_-) = \langle 01\Psi_- | \rho(6T) | 01\Psi_- \rangle,$$

$$P(\Phi_+) = \langle 10\Phi_+ | \rho(6T) | 10\Phi_+ \rangle,$$

$$P(\Phi_-) = \langle 11\Phi_- | \rho(6T) | 11\Phi_- \rangle, \quad (27)$$

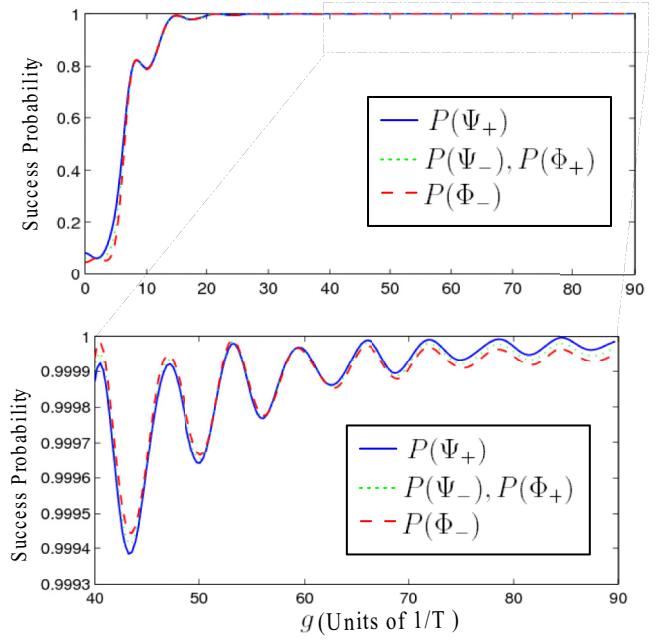
where

$$|00\Psi_+\rangle = |0\rangle_{A_1}|0\rangle_{A_2}|\Psi_+\rangle_{B_1B_2},$$

$$|01\Psi_-\rangle = |0\rangle_{A_1}|1\rangle_{A_2}|\Psi_-\rangle_{B_1B_2},$$

$$|10\Phi_+\rangle = |1\rangle_{A_1}|0\rangle_{A_2}|\Phi_+\rangle_{B_1B_2},$$

$$|11\Phi_-\rangle = |1\rangle_{A_1}|1\rangle_{A_2}|\Phi_-\rangle_{B_1B_2}. \quad (28)$$

FIG. 4. Success probabilities vs  $g$ .  $P(\Psi_+)$  (solid blue line),  $P(\Psi_-)$ ,  $P(\Phi_+)$  (dotted green line), and  $P(\Phi_-)$  (dashed red line).

First, as we perform the numerical simulation based on the original Hamiltonian shown in Eq. (5), a suitable coupling constant  $g$  should be chosen. Thus, we plot  $P(\Psi_+)$ ,  $P(\Psi_-)$ ,  $P(\Phi_+)$ , and  $P(\Phi_-)$  versus  $g$  in Fig. 4. As shown in Fig. 4, the success probability is very low when  $g$  is small due to bit flip errors, while they are near 1 when  $g \geq 30/T$ . According to Fig. 4, we choose  $g = 66/T$ , which gives  $\max\{|1 - P(\Psi_+)|, |1 - P(\Psi_-)|, |1 - P(\Phi_+)|, |1 - P(\Phi_-)|\} \leq 1.1847 \times 10^{-5}$ .

Second, we investigate the robustness of the protocol against decoherence. The main decoherent factors for the protocol are (1) cavity dissipations for cavity fields  $a_1$  and  $a_2$  with decay rates  $\kappa_1$  and  $\kappa_2$ , respectively; (2) spontaneous emissions from  $|3\rangle_{A_j}$  ( $|4\rangle_{A_j}$ ) to  $|0\rangle_{A_j}$ ,  $|1\rangle_{A_j}$  and  $|2\rangle_{A_j}$  with spontaneous-emission rates  $\gamma_{30A_j}$  ( $\gamma_{40A_j}$ ),  $\gamma_{31A_j}$  ( $\gamma_{41A_j}$ ), and  $\gamma_{32A_j}$  ( $\gamma_{42A_j}$ ), respectively; (3) spontaneous emissions from  $|2\rangle_{B_j}$  to  $|0\rangle_{B_j}$  and  $|1\rangle_{B_j}$  with spontaneous-emission rates  $\gamma_{20B_j}$  and  $\gamma_{21B_j}$ , respectively; (4) dephasings between  $|3\rangle_{A_j}$  ( $|4\rangle_{A_j}$ ) and  $|0\rangle_{A_j}$ ,  $|1\rangle_{A_j}$ ,  $|2\rangle_{A_j}$  with dephasing rates  $\gamma_{\phi30A_j}$  ( $\gamma_{\phi40A_j}$ ),  $\gamma_{\phi31A_j}$  ( $\gamma_{\phi41A_j}$ ), and  $\gamma_{\phi32A_j}$  ( $\gamma_{\phi42A_j}$ ), respectively; (5) dephasings between  $|2\rangle_{B_j}$  and  $|0\rangle_{B_j}$ ,  $|1\rangle_{B_j}$  with spontaneous-emission rates  $\gamma_{\phi20B_j}$ ,  $\gamma_{\phi21B_j}$ , respectively. Here, we neglect the spontaneous emission and dephasing between  $|4\rangle_{A_j}$  and  $|3\rangle_{A_j}$  and that between  $|2\rangle_{A_j}$  and  $|0\rangle_{A_j}$  ( $|1\rangle_{A_j}$ ) because they are much weaker than spontaneous emissions and dephasings between other levels of SQUID qubit  $A_j$ . Thus, the evolution of the system could be described using a master equation,

$$\dot{\rho}(t) = i[\rho(t), H(t)] + \sum_{p=1}^{34} \left[ L_p \rho L_p^\dagger - \frac{1}{2} (L_p^\dagger L_p \rho + \rho L_p^\dagger L_p) \right], \quad (29)$$

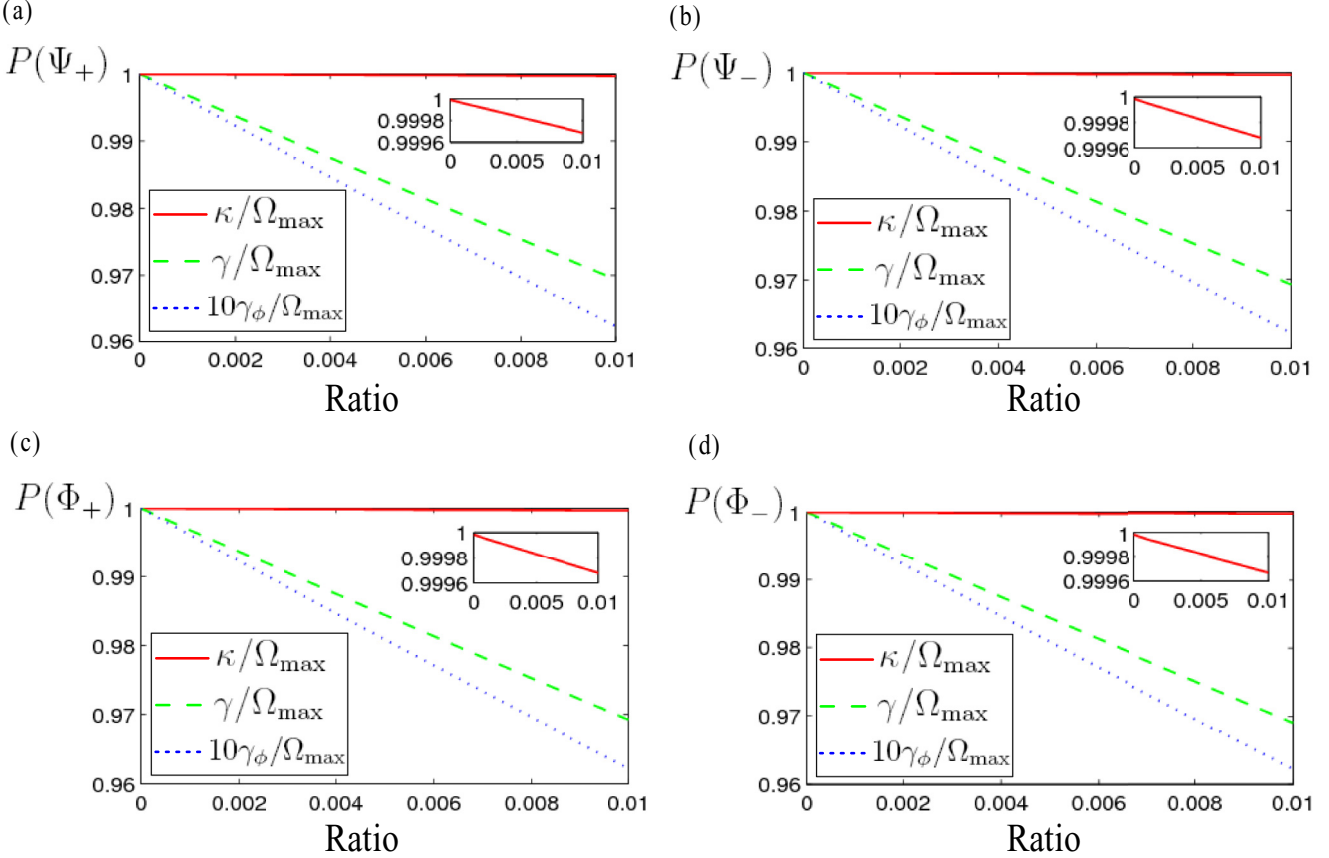


FIG. 5. (a)  $P(\Psi_+)$ , (b)  $P(\Psi_-)$ , (c)  $P(\Phi_+)$ , and (d)  $P(\Phi_-)$  vs  $\kappa/\Omega_{\max}$  (solid red line),  $\gamma/\Omega_{\max}$  (dashed green line), and  $10\gamma_\phi/\Omega_{\max}$  (dotted blue line).

where  $L_p$  ( $p = 1, 2, 3, \dots, 34$ ) is the Lindblad operator as

$$\begin{aligned}
 L_1 &= \sqrt{\gamma_{30A_1}}|0\rangle_{A_1}\langle 3|, \quad L_2 = \sqrt{\gamma_{31A_1}}|1\rangle_{A_1}\langle 3|, \quad L_3 = \sqrt{\gamma_{32A_1}}|2\rangle_{A_1}\langle 3|, \\
 L_4 &= \sqrt{\gamma_{40A_1}}|0\rangle_{A_1}\langle 4|, \quad L_5 = \sqrt{\gamma_{41A_1}}|1\rangle_{A_1}\langle 4|, \quad L_6 = \sqrt{\gamma_{42A_1}}|2\rangle_{A_1}\langle 4|, \\
 L_7 &= \sqrt{\gamma_{30A_2}}|0\rangle_{A_2}\langle 3|, \quad L_8 = \sqrt{\gamma_{31A_2}}|1\rangle_{A_2}\langle 3|, \quad L_9 = \sqrt{\gamma_{32A_2}}|2\rangle_{A_2}\langle 3|, \\
 L_{10} &= \sqrt{\gamma_{40A_2}}|0\rangle_{A_2}\langle 4|, \quad L_{11} = \sqrt{\gamma_{41A_2}}|1\rangle_{A_2}\langle 4|, \quad L_{12} = \sqrt{\gamma_{42A_2}}|2\rangle_{A_2}\langle 4|, \\
 L_{13} &= \sqrt{\gamma_{20B_1}}|0\rangle_{B_1}\langle 2|, \quad L_{14} = \sqrt{\gamma_{21B_1}}|1\rangle_{B_1}\langle 2|, \quad L_{15} = \sqrt{\gamma_{20B_2}}|0\rangle_{B_2}\langle 2|, \\
 L_{16} &= \sqrt{\gamma_{21B_2}}|1\rangle_{B_2}\langle 2|, \quad L_{17} = \sqrt{\kappa_1}a_1, \quad L_{18} = \sqrt{\kappa_2}a_2, \\
 L_{19} &= \sqrt{\gamma_{\phi30A_1}}(|3\rangle_{A_1}\langle 3| - |0\rangle_{A_1}\langle 0|), \quad L_{20} = \sqrt{\gamma_{\phi31A_1}}(|3\rangle_{A_1}\langle 3| - |1\rangle_{A_1}\langle 1|), \\
 L_{21} &= \sqrt{\gamma_{\phi32A_1}}(|3\rangle_{A_1}\langle 3| - |2\rangle_{A_1}\langle 2|), \quad L_{22} = \sqrt{\gamma_{\phi40A_1}}(|4\rangle_{A_1}\langle 4| - |0\rangle_{A_1}\langle 0|), \\
 L_{23} &= \sqrt{\gamma_{\phi41A_1}}(|4\rangle_{A_1}\langle 4| - |1\rangle_{A_1}\langle 1|), \quad L_{24} = \sqrt{\gamma_{\phi42A_1}}(|4\rangle_{A_1}\langle 4| - |2\rangle_{A_1}\langle 2|), \\
 L_{25} &= \sqrt{\gamma_{\phi30A_2}}(|3\rangle_{A_2}\langle 3| - |0\rangle_{A_2}\langle 0|), \quad L_{26} = \sqrt{\gamma_{\phi31A_2}}(|3\rangle_{A_2}\langle 3| - |1\rangle_{A_2}\langle 1|), \\
 L_{27} &= \sqrt{\gamma_{\phi32A_2}}(|3\rangle_{A_2}\langle 3| - |2\rangle_{A_2}\langle 2|), \quad L_{28} = \sqrt{\gamma_{\phi40A_2}}(|4\rangle_{A_2}\langle 4| - |0\rangle_{A_2}\langle 0|), \\
 L_{29} &= \sqrt{\gamma_{\phi41A_2}}(|4\rangle_{A_2}\langle 4| - |1\rangle_{A_2}\langle 1|), \quad L_{30} = \sqrt{\gamma_{\phi42A_2}}(|4\rangle_{A_2}\langle 4| - |2\rangle_{A_2}\langle 2|), \\
 L_{31} &= \sqrt{\gamma_{\phi20B_1}}(|2\rangle_{B_1}\langle 2| - |0\rangle_{B_1}\langle 0|), \quad L_{32} = \sqrt{\gamma_{\phi21B_1}}(|2\rangle_{B_1}\langle 2| - |1\rangle_{B_1}\langle 1|), \\
 L_{33} &= \sqrt{\gamma_{\phi20B_2}}(|2\rangle_{B_2}\langle 2| - |0\rangle_{B_2}\langle 0|), \quad L_{34} = \sqrt{\gamma_{\phi21B_2}}(|2\rangle_{B_2}\langle 2| - |1\rangle_{B_2}\langle 1|).
 \end{aligned} \tag{30}$$

For brief discussions, we assume  $\gamma_{30A_j} = \gamma_{31A_j} = \gamma_{32A_j} = \gamma_{40A_j} = \gamma_{41A_j} = \gamma_{42A_j} = \gamma_{20B_j} = \gamma_{21B_j} = \gamma$ ,  $\gamma_{\phi30A_j} = \gamma_{\phi31A_j} = \gamma_{\phi32A_j} = \gamma_{\phi40A_j} = \gamma_{\phi41A_j} = \gamma_{\phi42A_j} = \gamma_{\phi20B_j} = \gamma_{\phi21B_j} = \gamma_\phi$ ,  $\kappa_1 = \kappa_2 = \kappa$ .  $P(\Psi_+)$ ,  $P(\Psi_-)$ ,  $P(\Phi_+)$ , and

$P(\Phi_-)$  versus  $\gamma/\Omega_{\max}$ ,  $10\gamma_\phi/\Omega_{\max}$ , and  $\kappa/\Omega_{\max}$  are plotted in Figs. 5(a)–5(d), respectively.

As shown by Fig. 5, the Bell-state analysis is quite robust against the cavity decays. The success probabilities of

distinguishing each Bell state are still higher than 0.9996 when  $\kappa/\Omega_{\max} = 0.01$ . We can also find that the Bell-state analysis is more sensitive to the spontaneous emissions of SQUID qubits. When  $\gamma/\Omega_{\max} = 0.01$ , the success probabilities of distinguishing each Bell state are all a little less than 0.97. As for the dephasings, they are the most troublesome decoherent factors. When  $\gamma_\phi/\Omega_{\max} = 0.001$ , the success probabilities of distinguishing each Bell state are all higher than 0.96. We considered experimentally realizable parameters  $\Omega_{\max} = 2\pi \times 6.37$  MHz,  $g = 2\pi \times 85.14$  MHz,  $\kappa = 1.32$  MHz,  $\gamma = 0.40$  MHz,  $\gamma_\phi = 0.20$  MHz [37,38,55], and we have  $P(\Psi_+) = 0.9555$ ,  $P(\Psi_-) = 0.9554$ ,  $P(\Phi_+) = 0.9554$ , and  $P(\Phi_-) = 0.9554$ . Therefore, the protocol possesses a high success probability to distinguish each one of the four Bell states.

## VI. CONCLUSION

In conclusion, we have proposed a protocol for complete Bell-state analysis for superconducting-quantum-interference-device qubits. Although the Bell-state analysis is composed of six steps, one just needs to use a sequence of sinusoidal microwave pulses, as shown in Fig. 3, without any additional operations. Therefore, the operations are not difficult in experiments. After the six steps, the information for distinguishing four Bell states is encoded on two auxiliary qubits  $A_1$  and  $A_2$ . Thus, we can read out the information by detecting the states of

$A_1$  and  $A_2$ . The detections of SQUID qubits have been reported in protocols [93,94]. In this paper, we have not considered the detection efficiency, while for a real experiment, they should be taken into account. Moreover, apart from the advantages of SQUID qubits, the protocol holds some other advantages:

(1) The Bell-state analysis is complete and nondestructive. In other words, we can completely distinguish four Bell states without destroying them. Thus the physical resource could be saved.

(2) As shown by the numerical simulations, under the current experimental conditions, the protocol still possesses a high success probability of distinguishing each Bell state when decoherence is taken into account.

(3) Since STA is used in the pulse design, the operation speed of the protocol may be faster than that using the adiabatic passages.

Thus, we hope that the protocol contributes to information readout for quantum communications and quantum computations in superconducting quantum networks.

## ACKNOWLEDGMENTS

This work was supported by the National Natural Science Foundation of China under Grants No. 11575045, No. 11374054, and No. 11674060, and the Major State Basic Research Development Program of China under Grant No. 2012CB921601.

## APPENDIX: THE DERIVATION OF THE EFFECTIVE HAMILTONIAN

Here, we would like to amply describe the derivation of the effective Hamiltonian  $H_{\text{eff}1}(t)$  shown in Eq. (9) from Eqs. (7) and (8). According to the eigenstates of  $H_{c1}$  shown in Eq. (8), we can rewrite Eq. (7) as

$$\begin{aligned} H_{\text{step}1}(t) &= H_{m1}(t) + H_{c1}, \\ H_{m1}(t) &= \frac{\Omega_{03A_1}(t)}{\sqrt{2(g_{23A_1}^2 + g_{B_1}^2)}} |\bar{\psi}_1\rangle (\sqrt{2}g_{B1}\langle\bar{\phi}_0| + g_{23A_1}\langle\bar{\phi}_3| + g_{23A_1}\langle\bar{\phi}_4|) \\ &\quad + \frac{\Omega_{03A_1}(t)}{\sqrt{2}} |\bar{\psi}_6\rangle (\langle\bar{\phi}_1| + \langle\bar{\phi}_2|) + \frac{\Omega_{13A_1}(t)}{\sqrt{2}} |\bar{\psi}_9\rangle (\langle\bar{\phi}_1| + \langle\bar{\phi}_2|) \\ &\quad + \frac{\Omega_{13A_1}(t)}{\sqrt{2(g_{23A_1}^2 + g_{B_1}^2)}} |\bar{\psi}_5\rangle (\sqrt{2}g_{B1}\langle\bar{\phi}_0| + g_{23A_1}\langle\bar{\phi}_3| + g_{23A_1}\langle\bar{\phi}_4|) + \text{H.c.}, \\ H_{c1} &= g_{23A_1}(|\bar{\phi}_1\rangle\langle\bar{\phi}_1| - |\bar{\phi}_2\rangle\langle\bar{\phi}_2|) + \sqrt{g_{23A_1}^2 + g_{B_1}^2} (|\bar{\phi}_3\rangle\langle\bar{\phi}_3| - |\bar{\phi}_4\rangle\langle\bar{\phi}_4|). \end{aligned} \quad (\text{A1})$$

Considering  $H_{c1}$  as a free Hamiltonian, we perform the picture transformation  $\bar{U} = e^{-iH_{c1}t}$  on Eq. (A1). The Hamiltonian after the transformation is

$$\begin{aligned} H'_{\text{step}1}(t) &= \frac{\Omega_{03A_1}(t)}{\sqrt{2(g_{23A_1}^2 + g_{B_1}^2)}} |\bar{\psi}_1\rangle (\sqrt{2}g_{B1}\langle\bar{\phi}_0| + g_{23A_1}\langle\bar{\phi}_3|e^{-i\sqrt{g_{23A_1}^2 + g_{B_1}^2}t} + g_{23A_1}\langle\bar{\phi}_4|e^{i\sqrt{g_{23A_1}^2 + g_{B_1}^2}t}) \\ &\quad + \frac{\Omega_{13A_1}(t)}{\sqrt{2(g_{23A_1}^2 + g_{B_1}^2)}} |\bar{\psi}_5\rangle (\sqrt{2}g_{B1}\langle\bar{\phi}_0| + g_{23A_1}\langle\bar{\phi}_3|e^{-i\sqrt{g_{23A_1}^2 + g_{B_1}^2}t} + g_{23A_1}\langle\bar{\phi}_4|e^{i\sqrt{g_{23A_1}^2 + g_{B_1}^2}t}) \\ &\quad + \frac{\Omega_{03A_1}(t)}{\sqrt{2}} |\bar{\psi}_6\rangle (\langle\bar{\phi}_1|e^{-ig_{23A_1}t} + \langle\bar{\phi}_2|e^{ig_{23A_1}t}) + \frac{\Omega_{13A_1}(t)}{\sqrt{2}} |\bar{\psi}_9\rangle (\langle\bar{\phi}_1|e^{-ig_{23A_1}t} + \langle\bar{\phi}_2|e^{ig_{23A_1}t}) + \text{H.c.} \end{aligned} \quad (\text{A2})$$

Under the condition  $\Omega_{03A_1}(t), \Omega_{13A_1}(t) \ll g_{23A_1}, g_{B_1}$ , we neglect the terms of high-frequency oscillations and obtain the effective Hamiltonian,

$$H_{\text{eff}1}(t) = \frac{g_{B_1}}{\sqrt{g_{23A_1}^2 + g_{B_1}^2}} [\Omega_{03A_1}(t)|\bar{\psi}_1\rangle\langle\bar{\phi}_0| + \Omega_{13A_1}(t)|\bar{\psi}_5\rangle\langle\bar{\phi}_0|] + \text{H.c.} \quad (\text{A3})$$

In a similar way, we can derive the effective Hamiltonian  $H_{\text{eff}2}(t)$  shown in Eq. (11) from Eqs. (9) and (10).

- 
- [1] J. S. Bell, *Physics* **1**, 195 (1964).
- [2] D. M. Greenberger, M. A. Horne, and A. Zeilinger, in *Bell's Theorem, Quantum Theory, and Conceptions of the Universe*, edited by M. Kafatos (Kluwer, Dordrecht, 1989), p. 69.
- [3] W. Dür, G. Vidal, and J. I. Cirac, *Phys. Rev. A* **62**, 062314 (2000).
- [4] A. Karlsson and M. Bourennane, *Phys. Rev. A* **58**, 4394 (1998).
- [5] F. G. Deng, X. H. Li, C. Y. Li, P. Zhou, and H. Y. Zhou, *Phys. Rev. A* **72**, 044301 (2005).
- [6] A. K. Ekert, *Phys. Rev. Lett.* **67**, 661 (1991).
- [7] F. G. Deng, G. L. Long, and X. S. Liu, *Phys. Rev. A* **68**, 042317 (2003).
- [8] C. H. Bennett and S. J. Wiesner, *Phys. Rev. Lett.* **69**, 2881 (1992).
- [9] X. S. Liu, G. L. Long, D. M. Tong, and L. Feng, *Phys. Rev. A* **65**, 022304 (2002).
- [10] Y. B. Sheng and F. G. Deng, *Phys. Rev. A* **81**, 042332 (2010).
- [11] Z. J. Deng, K. L. Gao, and M. Feng, *Phys. Rev. A* **74**, 064303 (2006).
- [12] L. M. Duan and H. J. Kimble, *Phys. Rev. Lett.* **90**, 253601 (2003).
- [13] T. J. Wang, S. Y. Song, and G. L. Long, *Phys. Rev. A* **85**, 062311 (2012).
- [14] C. Y. Hu and J. G. Rarity, *Phys. Rev. B* **83**, 115303 (2011).
- [15] B. C. Ren, F. F. Du, and F. G. Deng, *Phys. Rev. A* **90**, 052309 (2014).
- [16] J. W. Pan, C. Simon, Č. Brukner, and A. Zeilinger, *Nature (London)* **410**, 1067 (2001).
- [17] C. H. Bennett, G. Brassard, and N. D. Mermin, *Phys. Rev. Lett.* **68**, 557 (1992).
- [18] K. Mattle, H. Weinfurter, P. G. Kwiat, and A. Zeilinger, *Phys. Rev. Lett.* **76**, 4656 (1996).
- [19] J. A. W. van Houwelingen, N. Brunner, A. Beveratos, H. Zbinden, and N. Gisin, *Phys. Rev. Lett.* **96**, 130502 (2006).
- [20] L. Vaidman and N. Yoran, *Phys. Rev. A* **59**, 116 (1999).
- [21] J. Calsamiglia, *Phys. Rev. A* **65**, 030301(R) (2002).
- [22] M. Barbieri, G. Vallone, P. Mataloni, and F. De Martini, *Phys. Rev. A* **75**, 042317 (2007).
- [23] Y. B. Sheng and F. G. Deng, *Phys. Rev. A* **81**, 032307 (2010).
- [24] Y. B. Sheng, F. G. Deng, and G. L. Long, *Phys. Rev. A* **82**, 032318 (2010).
- [25] T. J. Wang, Y. Lu, and G. L. Long, *Phys. Rev. A* **86**, 042337 (2012).
- [26] B. C. Ren, H. R. Wei, M. Hua, T. Li, and F. G. Deng, *Opt. Express* **20**, 24664 (2012).
- [27] C. Bonato, F. Haupt, S. S. R. Oemrawsingh, J. Gudat, D. Ding, M. P. van Exter, and D. Bouwmeester, *Phys. Rev. Lett.* **104**, 160503 (2010).
- [28] Y. Xia, Y. H. Kang, and P. M. Lu, *J. Opt. Soc. Am. B* **31**, 2077 (2014).
- [29] Y. He and N. Q. Jiang, *Chin. Phys. B* **19**, 099702 (2010).
- [30] H. R. Wei, B. C. Ren, M. Zhang, T. Li, and F. G. Deng, *Int. J. Theor. Phys.* **52**, 4045 (2013).
- [31] Y. H. Kang, Y. Xia, and P. M. Lu, *Appl. Phys. B* **119**, 259 (2015).
- [32] J. Z. Lin, *Int. J. Theor. Phys.* **56**, 456 (2017).
- [33] Y. Makhlin, G. Schön, and A. Shnirman, *Rev. Mod. Phys.* **73**, 357 (2001).
- [34] A. Steinbach, P. Joyez, A. Cottet, D. Esteve, M. H. Devoret, M. E. Huber, and J. M. Martinis, *Phys. Rev. Lett.* **87**, 137003 (2001).
- [35] D. Vion, A. Aassime, A. Cottet, P. Joyez, H. Pothier, C. Urbina, D. Esteve, and M. H. Devoret, *Science* **296**, 886 (2002).
- [36] Y. Yu, S. Han, X. Chu, S.-I Chu, and Z. Wang, *Science* **296**, 889 (2002).
- [37] C. P. Yang, S.-I Chu, and S. Han, *Phys. Rev. Lett.* **92**, 117902 (2004).
- [38] C. P. Yang, S.-I Chu, and S. Han, *Phys. Rev. A* **67**, 042311 (2003).
- [39] I. Chiorescu, P. Bertet, K. Semba, Y. Nakamura, C. J. P. M. Harmans, and J. E. Mooij, *Nature (London)* **431**, 159 (2004).
- [40] A. Blais, R. S. Huang, A. Wallraff, S. M. Girvin, and R. J. Schoelkopf, *Phys. Rev. A* **69**, 062320 (2004).
- [41] A. Wallraff, D. I. Schuster, A. Blais, L. Frunzio, R. S. Huang, J. Majer, S. Kumar, S. M. Girvin, and R. J. Schoelkopf, *Nature (London)* **431**, 162 (2004).
- [42] C. P. Yang and S. Han, *Phys. Rev. A* **74**, 044302 (2006).
- [43] J. Koch, T. M. Yu, J. Gambetta, A. A. Houck, D. I. Schuster, J. Majer, A. Blais, M. H. Devoret, S. M. Girvin, and R. J. Schoelkopf, *Phys. Rev. A* **76**, 042319 (2007).
- [44] J. Majer, J. M. Chow, J. M. Gambetta, J. Koch, B. R. Johnson, J. A. Schreier, L. Frunzio, D. I. Schuster, A. A. Houck, A. Wallraff, A. Blais, M. H. Devoret, S. M. Girvin, and R. J. Schoelkopf, *Nature (London)* **449**, 443 (2007).
- [45] M. H. Devoret, S. Girvin, and R. Schoelkopf, *Ann. Phys. (Leipzig)* **16**, 767 (2007).
- [46] J. Clarke and F. K. Wilhelm, *Nature (London)* **453**, 1031 (2008).
- [47] L. DiCarlo, J. M. Chow, J. M. Gambetta, L. S. Bishop, B. R. Johnson, D. I. Schuster, J. Majer, A. Blais, L. Frunzio, S. M. Girvin, and R. J. Schoelkopf, *Nature (London)* **460**, 240 (2009).
- [48] S. Filipp, P. Maurer, P. J. Leek, M. Baur, R. Bianchetti, J. M. Fink, M. Göppel, L. Steffen, J. M. Gambetta, A. Blais, and A. Wallraff, *Phys. Rev. Lett.* **102**, 200402 (2009).
- [49] C. P. Yang, *Phys. Rev. A* **82**, 054303 (2010).
- [50] R. C. Bialczak, M. Ansmann, M. Hofheinz, E. Lucero, M. Neeley, A. D. O'Connell, D. Sank, H. Wang, J. Wenner, M. Steffen, A. N. Cleland, and J. M. Martinis, *Nat. Phys.* **6**, 409 (2010).

- [51] T. Yamamoto, M. Neeley, E. Lucero, R. C. Bialczak, J. Kelly, M. Lenander, M. Mariantoni, A. D. O’Connell, D. Sank, H. Wang, M. Weides, J. Wenner, Y. Yin, A. N. Cleland, and J. M. Martinis, *Phys. Rev. B* **82**, 184515 (2010).
- [52] M. D. Reed, L. DiCarlo, B. R. Johnson, L. Sun, D. I. Schuster, L. Frunzio, and R. J. Schoelkopf, *Phys. Rev. Lett.* **105**, 173601 (2010).
- [53] F. W. Strauch, K. Jacobs, and R. W. Simmonds, *Phys. Rev. Lett.* **105**, 050501 (2010).
- [54] C. P. Yang, Q. P. Su, and S. Han, *Phys. Rev. A* **86**, 022329 (2012).
- [55] Z. L. Xiang, S. Ashhab, J. Q. You, and F. Nori, *Rev. Mod. Phys.* **85**, 623 (2013).
- [56] C. P. Yang, Q. P. Su, S. B. Zheng, and S. Han, *Phys. Rev. A* **87**, 022320 (2013).
- [57] S. Schmidt and J. Koch, *Ann. Phys.* **525**, 395 (2013).
- [58] K. H. Song, S. H. Xiang, Q. Liu, and D. H. Lu, *Phys. Rev. A* **75**, 032347 (2007).
- [59] M. V. Berry, *J. Phys. A* **42**, 365303 (2009).
- [60] X. Chen, I. Lizuain, A. Ruschhaupt, D. Guéry-Odelin, and J. G. Muga, *Phys. Rev. Lett.* **105**, 123003 (2010).
- [61] A. del Campo, *Phys. Rev. Lett.* **111**, 100502 (2013).
- [62] Y. H. Chen, Q. C. Wu, B. H. Huang, J. Song, and Y. Xia, *Sci. Rep.* **6**, 38484 (2016).
- [63] X. Chen, E. Torrontegui, and J. G. Muga, *Phys. Rev. A* **83**, 062116 (2011).
- [64] A. del Campo, M. M. Rams, and W. H. Zurek, *Phys. Rev. Lett.* **109**, 115703 (2012).
- [65] X. Chen, A. Ruschhaupt, S. Schmidt, A. del Campo, D. Guéry-Odelin, and J. G. Muga, *Phys. Rev. Lett.* **104**, 063002 (2010).
- [66] E. Torrontegui, S. Ibáñez, S. Martínez-Garaot, M. Modugno, A. del Campo, D. Guéry-Odelin, A. Ruschhaupt, X. Chen, and J. G. Muga, *Adv. At. Mol. Opt. Phys.* **62**, 117 (2013).
- [67] J. G. Muga, X. Chen, A. Ruschhaupt, and D. Guéry-Odelin, *J. Phys. B* **42**, 241001 (2009).
- [68] A. del Campo and M. G. Boshier, *Sci. Rep.* **2**, 648 (2012).
- [69] S. Martínez-Garaot, E. Torrontegui, X. Chen, and J. G. Muga, *Phys. Rev. A* **89**, 053408 (2014).
- [70] E. Torrontegui, S. Martínez-Garaot, and J. G. Muga, *Phys. Rev. A* **89**, 043408 (2014).
- [71] H. Saberi, T. Opatrný, K. Mølmer, and A. del Campo, *Phys. Rev. A* **90**, 060301(R) (2014).
- [72] B. T. Torosov, G. DellaValle, and S. Longhi, *Phys. Rev. A* **87**, 052502 (2013).
- [73] B. T. Torosov, G. DellaValle, and S. Longhi, *Phys. Rev. A* **89**, 063412 (2014).
- [74] S. Ibáñez, X. Chen, E. Torrontegui, J. G. Muga, and A. Ruschhaupt, *Phys. Rev. Lett.* **109**, 100403 (2012).
- [75] S. Ibáñez, X. Chen, and J. G. Muga, *Phys. Rev. A* **87**, 043402 (2013).
- [76] X. K. Song, Q. Ai, J. Qiu, and F. G. Deng, *Phys. Rev. A* **93**, 052324 (2016).
- [77] A. Baksic, H. Ribeiro, and A. A. Clerk, *Phys. Rev. Lett.* **116**, 230503 (2016).
- [78] E. Torrontegui, S. Ibáñez, X. Chen, A. Ruschhaupt, D. Guéry-Odelin, and J. G. Muga, *Phys. Rev. A* **83**, 013415 (2011).
- [79] J. G. Muga, X. Chen, S. Ibáñez, I. Lizuain, and A. Ruschhaupt, *J. Phys. B* **43**, 085509 (2010).
- [80] E. Torrontegui, X. Chen, M. Modugno, A. Ruschhaupt, D. Guéry-Odelin, and J. G. Muga, *Phys. Rev. A* **85**, 033605 (2012).
- [81] S. Masuda and K. Nakamura, *Phys. Rev. A* **84**, 043434 (2011).
- [82] S. Masuda and S. A. Rice, *J. Phys. Chem. A* **119**, 3479 (2015).
- [83] X. Chen and J. G. Muga, *Phys. Rev. A* **82**, 053403 (2010).
- [84] X. Chen, E. Torrontegui, D. Stefanatos, J. S. Li, and J. G. Muga, *Phys. Rev. A* **84**, 043415 (2011).
- [85] A. del Campo, *Eur. Phys. Lett.* **96**, 60005 (2011).
- [86] J. F. Schaff, X. L. Song, P. Vignolo, and G. Labeyrie, *Phys. Rev. A* **82**, 033430 (2010).
- [87] X. Chen and J. G. Muga, *Phys. Rev. A* **86**, 033405 (2012).
- [88] A. C. Santos, R. D. Silva, and M. S. Sarandy, *Phys. Rev. A* **93**, 012311 (2016).
- [89] I. Hen, *Phys. Rev. A* **91**, 022309 (2015).
- [90] S. Deffner, C. Jarzynski, and A. del Campo, *Phys. Rev. X* **4**, 021013 (2014).
- [91] A. del Campo, *Phys. Rev. A* **84**, 031606(R) (2011).
- [92] X. K. Song, H. Zhang, Q. Ai, J. Qiu, and F. G. Deng, *New J. Phys.* **18**, 023001 (2016).
- [93] D. A. Bennett, L. Longobardi, V. Patel, W. Chen, and J. E. Lukens, *Supercond. Sci. Technol.* **20**, S445 (2007).
- [94] H. Takayanagi, H. Tanaka, S. Saito, and H. Nakano, *Superlattice Microst.* **32**, 221 (2002).